PRELIMINARY RESULTS ON THE RETRIEVAL OF LAND SURFACE TEMPERATURE FROM MSG-SEVIRI DATA IN EASTERN SPAIN

Raquel Niclòs[1], Jose A. Valiente[1], Maria J. Barberà[1], Maria J. Estrela[2], Joan M. Galve[3], and Vicente Caselles[3]

[1] Unidad Mixta CEAM-UVEG. Fundación Centro de Estudios Ambientales del Mediterráneo (CEAM). Charles Darwin, 14, 46980 Paterna, SPAIN. niclos@ceam.es
[2] Unidad Mixta CEAM-UVEG. Departamento de Geografía. Universidad de Valencia (UVEG). Blasco Ibáñez, 28. 46010 Valencia, SPAIN.
[3]Dep. Física de la Tierra y Termodinámica. Universidad de Valencia (UVEG). Dr. Moliner, 50. 46100 Burjassot, SPAIN.

Abstract

A preliminary comparison between the Land Surface Temperature (LST) product generated by the LSA SAF and ground measurements carried out in an extensive, flat, unstressed, fully-covering rice field site showed an LST error larger than ±2K. Since then, several issues have been investigated with the aim of reducing error sources in the retrieval of LST from MSG-SEVIRI in Eastern Spain: a) a methodology to generate periodic and regional land cover maps has been suggested after observing classification errors in the land cover maps used by the LSA SAF to estimate surface emissivities, b) angular measurements of surface emission have been carried out to study the angular emission behaviour of land surfaces, which can have a significant effect on LST retrievals at off-nadir viewings, c) an alternative algorithm has been proposed for retrieving LST from MSG-SEVIRI data, and, finally, d) two ground-truth stations have been set up to evaluate the soundness of the LST algorithms.

INTRODUCTION

A frequent and accurate determination of Land Surface Temperature (LST) could help to improve the forecasting of natural hazards, such as extreme temperatures. The Spinning Enhanced Visible and Infrared Imager (SEVIRI) on board the geostationary METEOSAT Second Generation (MSG) platforms offers this possibility, since it has global coverage and a temporal resolution of 15 minutes. Nevertheless, a preliminary comparison between the LST product generated by the LSA SAF (Land Surface Analysis of the Satellite Application Facility) and ground-truth measurements carried out in a extensive, flat, unstressed and homogeneous rice crop area in Eastern Spain, which has been used as a satellite validation site in recent years (Coll et al. 2005), showed a bias and a standard deviation of 3K and ±1.4K, respectively. These results pointed out the need for a study on potential error sources to improve the LST retrieval from MSG-SEVIRI data.

One error source could be the land cover type classification used in the land cover maps adopted by the LSA SAF to estimate the surface emissivity required for the LST algorithm. Furthermore, the angular behaviour of surface emission should also be investigated for different land covers, since it could have important effects on LST due to the large range of observation angles used by the MSG-SEVIRI. Additionally, the soundness of the LSA SAF LST algorithm itself could be evaluated and compared with the results of other atmospheric and emissivity correction techniques. Two ground-truth validation sites have been set up in Eastern Spain to validate LST algorithms.

This work shows the first results of the research carried out to address the above issues with the aim of improving the determination of LST from MSG-SEVIRI imagery in Eastern Spain.

LAND COVER CLASSIFICATION

Because LST split-window algorithms require an estimate of surface emissivity as an input (see LST algorithms in the following sections), identifying the land cover type for each pixel is an important

matter. Nevertheless, some classification errors have been observed for the land cover maps used by the LSA SAF to estimate surface emissivity. For example, the 12ha rice crop area used for testing the LSA SAF LST product is incorrectly classified as evergreen needleaf forest (*International Geosphere-Biosphere Programme*, IGBP class 1).

Instead of using these maps, we suggest a periodic generation of regional land cover maps by means of a supervised classification method (maximum likelihood) based on the selection of representative and tested CORINE polygons (CEC, 1995) as ground-truth areas and the use of spectral images (bands 1-7) of the isotropic BRDF parameter given by the MODIS 16-day MCD43A1 product. The selected CORINE polygons were tested against in situ observations and orthophotographs. The isotropic BRDF parameter is independent of the observation and illumination angles and makes the resulting classification images intercomparable. The analysis of the confusion matrix between the generated classification images and ground-truth areas gave overall training and validation accuracies of 80% and 70%, respectively (Niclòs et al. 2009).

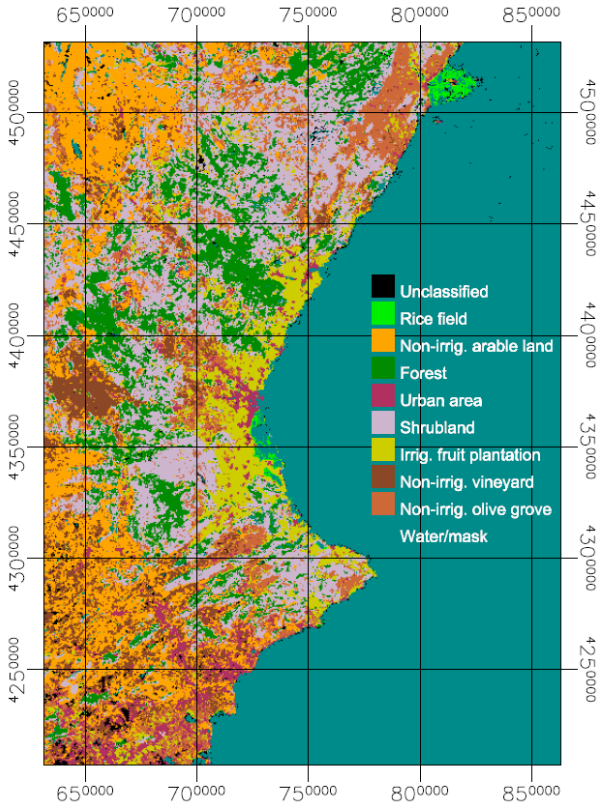

Figure 1: **Land cover map generated for Eastern Spain in August 2007 (UTM, European 1950, 30N).**

ANGULAR BEHAVIOUR OF SURFACE EMISSION

A mobile goniometric system was designed to measure the angular behaviour of surface emission during cloud-free sky conditions. This goniometric system allows a specific target area to be observed at different viewing angles by modifying the vertical and horizontal distances to the measurement point while the angle is changed by a graduated head (Figure 2a). An Apogee SI-111 (IRR-PN) radiometer (www.apogee-inst.com) is used to measure the angular variation of surface emission by using this goniometer. The atmospheric downwelling radiance is measured simultaneously with the surface emission, and the following equation is used to determine the relative emissivity to the nadir value, ε_{rel}, from these measurements:

$$\varepsilon_{rel}(\theta) = \frac{\varepsilon(\theta)}{\varepsilon(0^\circ)} = \frac{B(T_{rad}(\theta)) - B(T_{atm})}{B(T_{rad}(0^\circ)) - B(T_{atm})} = \frac{\exp(-\alpha / T_{rad}(\theta)) - \gamma \exp(-\alpha / T_{atm}(0^\circ))}{\exp(-\alpha / T_{rad}(0^\circ)) - \gamma \exp(-\alpha / T_{atm}(0^\circ))} \quad (1)$$

where ε(θ) and ε(0º) are the emissivities at zenith angles of θ and 0º (nadir), B is the Planck's function and T_{rad} and T_{atm} are the measured surface and atmospheric brightness temperatures. α=14388/λ, λ being the radiometer band wavelength (11.05μm), and *γ* is the ratio between the atmospheric downwelling irradiance and the atmospheric downwelling radiance at zenith, according to the diffusive approximation for cloud-free skies, which is 1.3 for the radiometer used (Niclòs et al. 2005).

Figure 2b shows the results obtained for two samples: a) an unstressed, fully-covering rice field and b) bare soil (clavisol). The rice emission shows no significant angular variation, thus agreeing with the measurements carried out by Lagourde et al. (1995) for an alfalfa crop in similar conditions. Such a small variation is attributed to the high density of the canopy (the soil was not visible) and the absence of water stress, which are likely to reduce the angular effects. Nevertheless, the bare soil shows a relative dependence on angle. This angular dependence should be taken into account in the determination of the pixel emissivities that use the algorithms to retrieve LST from satellite data, mainly for the pixels observed at large viewing angles, which is the case of most of Europe.

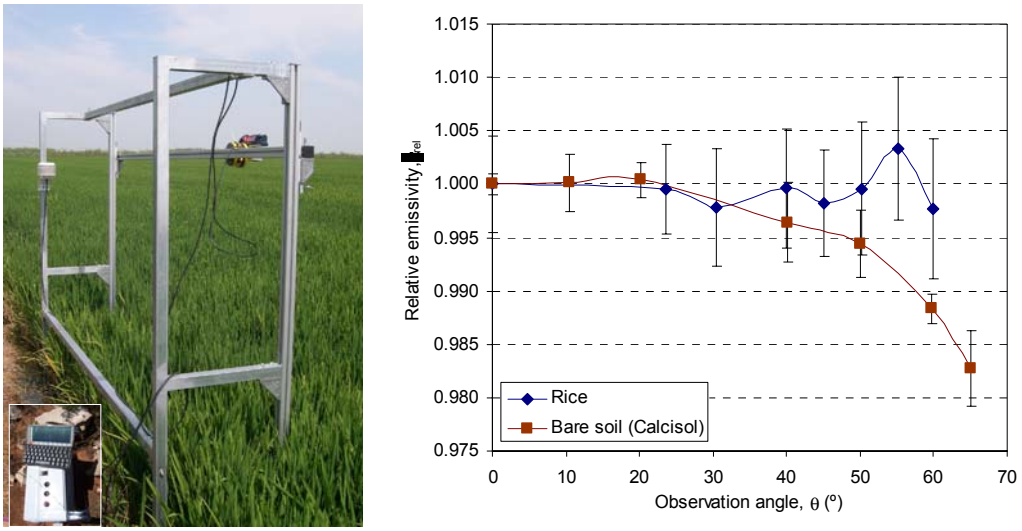

Figure 2: **(a) Goniometric system designed by the CEAM Team, and (b) Angular variation of the emissivity measured using the goniometer for two samples (rice and bare soil).**

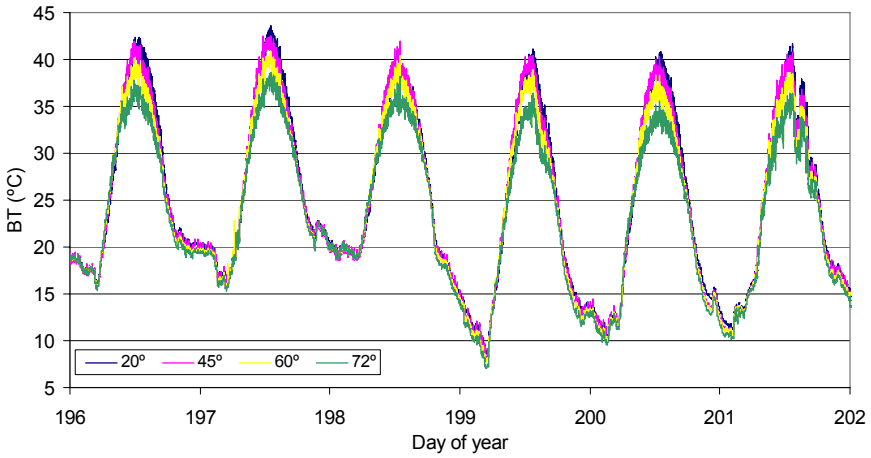

Figure 3: **Example of the brightness temperatures, BT, measured at the 4 different observation angles (6 days in 2009).**

Additionally, 4 Apogee SI-111 (IRR-PN) radiometers mounted on a meteorological tower have been measuring brightness temperature, BT, continuously at 4 different angles (20, 45, 60, 72º) in an extense, high-plain, homogeneous area of scrubland (see description in the following sections). Figure 3 shows a six-day example of the BTs measured at these angles. Figure 4 shows the effect of the viewing angle on the BT, with respect to the measurements carried out at the minimum angle (20º) at

two times of the day: at the time of maximum and minimum temperatures. In this case, as the sample is a combination of vegetation and bare ground, the angular dependence shown must be mainly due to the change in the fraction of vegetation cover seen at each angle. This fact can explain the smaller angular variation observed at UTC 4-5 (time of minimum temperatures) as compared to the one at UTC 13-14 (time of maximum temperatures), since in the second case the temperature difference between bare ground and vegetation is larger, and thus the effect of the FVC increase with angle is stronger.

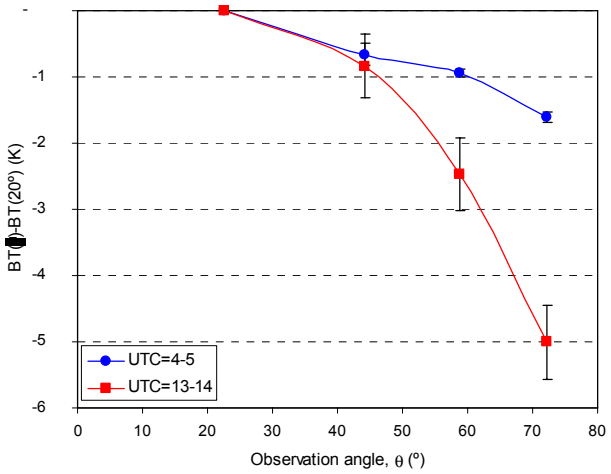

Figure 4: **Angular variation of BT measured on a cloud-free day (199 of 2009) at times of minimum (UTC 4-5) and maximum (UTC 13-14) temperatures.**

LST ALGORITHMS

LSA SAF LST product

The LSA SAF LST is estimated using a Generalized Split-Window (GSW) algorithm (Madeira 2002) that follows the formulation first proposed by Wan and Dozier (1996) for AVHRR and MODIS data. The LST is a function of the cloud-free top-of-atmosphere BTs measured by the MSG-SEVIRI 9 and 10 channels, centred at 10.8μm and 12μm, respectively, following the equation:

$$LST = (A_1 + A_2 \frac{1-\varepsilon}{\varepsilon} + A_3 \frac{\Delta\varepsilon}{\varepsilon^2}) \frac{T_9 + T_{10}}{2} + (B_1 + B_2 \frac{1-\varepsilon}{\varepsilon} + B_3 \frac{\Delta\varepsilon}{\varepsilon^2}) \frac{T_9 - T_{10}}{2} + C \quad (2)$$

where $\varepsilon = \frac{\varepsilon_9 + \varepsilon_{10}}{2}$ and $\Delta\varepsilon = \varepsilon_9 - \varepsilon_{10}$, and T_i and ε_i are the brightness temperatures and emissivities in the split-window channels 9 and 10. The A_1, A_2, A_3, B_1, B_2, B_3, C coefficients were obtained by regression using synthetic BTs simulated with the MODTRAN 4 code for 40 cloud-free TIGR-like atmospheric profiles and 50 radiosoundings covering a wide range of atmospheric conditions. According to the authors, these coefficients were estimated for classes of total column water vapour, W_0, and satellite zenith view angles, θ, and a look-up-table was generated with the obtained values. The W_0 required to select the most suitable coefficients is routinely obtained from the European Centre for Medium-Range Weather Forecast (ECMWF). Emissivities are operationally computed as $\varepsilon_i = \varepsilon_{i,v} FVC + \varepsilon_{i,bg}(1 - FVC)$, where the FVC is obtained from the LSA SAF FVC product (García-Haro et al. 2005) and the vegetation and bareground emissivities were previously assigned to each class on a land cover map used as reference (Trigo et al. 2008).

Proposed LST algorithm

In this work, we also suggest a quadratic split-window equation that follows the expression proposed by Coll and Caselles (1997), which incorporates separate terms for the atmospheric and emissivity corrections. This algorithm can be written as:

$$LST = T_9 + a\,(T_9-T_{10}) + b\,(T_9-T_{10})^2 + c + B(\varepsilon) \quad (3)$$

where a, b and c are the atmospheric coefficients, which are independent of the surface properties (Coll and Caselles, 1997). Emissivity effects are compensated by the term B(ε). This term depends on the average surface emissivity, ε, and the difference, Δε, for both split-window channels, as follows:

$$B(\varepsilon)=\alpha(1-\varepsilon)-\beta\Delta\varepsilon \quad (4)$$

where α and β depend both on the atmospheric properties, so as to characterise the reflection of the downwelling sky radiance, and on the surface temperature (Coll and Caselles, 1997).

A set of 382 global land atmospheric radiosoundings uniformly distributed at global scale were used to generate the synthetic BTs required to obtain the algorithm coefficients. This set of atmospheric profiles was collected from the Atmospheric Science Department-University of Wyoming (http:// weather.uwyo.edu/upperair/sounding.html) in order to have a distribution of cloud-free data uniform with W_0, latitude and surface temperature (Galve et al. 2008). BTs for the MSG-SEVIRI split-window channels were simulated by using this dataset and the MODTRAN 4.0 code. Seven surface temperatures were considered for each atmospheric profile: T_0-6K, T_0-2K, T_0+1K, T_0+3K, T_0+5K, T_0+8K, T_0+12K, with T_0 being the temperature of the first layer of each atmospheric profile (Galve et al. 2008).

Atmospheric surface-independent coefficients (a, b, and c) were calculated for MSG-SEVIRIs by means of a regression analysis between LST-T_9 and T_9-T_{10} when the top-of-atmosphere BTs wereobtained by considering ε =1 and Δε =0 (Coll and Caselles 1997). The atmospheric correction required for a given atmospheric profile increases with the observation angle, θ, as a consequence of the atmospheric path enlargement (i.e., the optical path increases by a factor sec(θ)-1). Taking into account the higher increase in LST-T_9 than in T_9-T_{10} with angle, an angular dependence of the atmospheric coefficients is required to fit these differences at any angle (Niclos et al. 2007, Niclos et al. 2008). The regressions obtained from the simulations showed that a and b can be expressed as a linear function of sec(θ)-1.

As coefficients α and β in the emissivity term depend on atmospheric properties (Coll and Caselles 1997), they should also depend on W_0 (Niclos et al. 2008). In this case, a quadratic expression with the oblique water vapour, $W= W_0/\cos(\theta)$, was obtained for α and a linear dependence was observed for β.

Finally, the proposed expression can be written from equations (3)-(4) as:

$$LST= T_9 + a(S)\,(T_9-T_{10}) + b(S)\,(T_9-T_{10})^2 + c + \alpha(W)\,(1-\varepsilon) - \beta(W)\,\Delta\varepsilon \quad (5)$$

where all the temperatures are in degrees Kelvin, $a(S)=(a_0+a_1S)$, $b(S)=(b_0+b_1S)$, $\alpha(W)=(\alpha_0+\alpha_1W+\alpha_2W^2)$, and $\beta(W)=(\beta_0+\beta_1W)$; S and W are S=sec(θ)-1 and $W=W_0/\cos(\theta)$ (in cm^{-1}), respectively. The coefficients for the SEVIRI sensor in MSG-2 are given in Table 1.

a_0	1.04±0.03
a_1	0.13±0.04
b_0 (K^{-1})	0.249±0.006
b_1 (K^{-1})	0.135±0.008
c (K)	0.32±0.04
α_0 (K)	51.07±0.18
α_1 (K cm^{-1})	0.47±0.13
α_2 (K cm^{-2})	-1.049±0.019
β_0 (K)	95.2±0.2
β_1 (K cm^{-1})	-14.26±0.06

Table 1: **Coefficients of the proposed equation for the SEVIRI sensor on MSG-2.**

GROUND-TRUTH DATA AND VALIDATION

Two ground-truth validation stations have been set up in Eastern Spain to validate LST algorithms and study the relationship between LST and surface air temperature. One of these is located in a large, high-plain, homogeneous area of scrubland (zone A; WGS-84, 39.224N, -0.903E) dominated by rosemary (*Rosmarinus officinalis* L.) and gorse (*Ulex parviflorus* L.), i.e., the typical Mediterranean calcic thermophile scrubland and one of the most representative natural canopies in Eastern Spain. The FVC is 0.49 for a nadir view in this area. The second station is located in an extense and homogeneous area of rice-crop fields (zone B; WGS-84, 39.224ºN, -0.903ºE). This area has a FVC close to 1 from June to September, when thermal measurements are useful for validation (Figure 6).

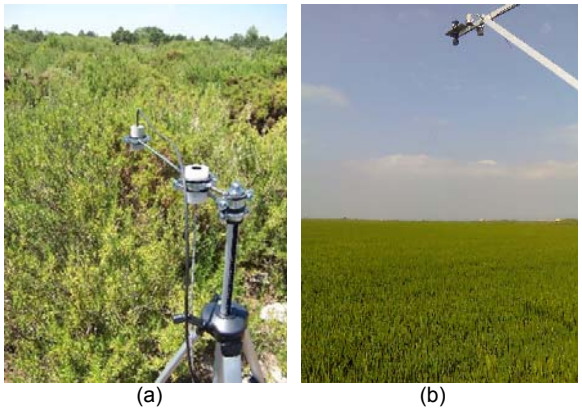

(a) (b)

Figure 6: **Zones A and B: (a) Mediterranean calcic thermophile scrubland, and (b) rice-crop fields.**

These two stations were equipped with Apogee SI-111/SI-121 (IRR-PN/P) thermal-infrared radiometers and complete meteorological stations for measuring solar irradiance, air temperature, wind speed, etc. The Apogee radiometers were calibrated against a NIST blackbody obtaining a BT accuracy of ±0.2K at 293K (CEOS, Committee on Earth Observation Satellites, IR comparison). The radiance measured by a radiometer observing the surface can be expressed as:

$$R = \varepsilon\ B(LST) + (1-\varepsilon)\ L^{\downarrow}_{atm\ hem} \qquad (6)$$

where the downwelling atmospheric irradiance, $L^{\downarrow}_{atm\ hem}$, is measured simultaneously by a second radiometer observing at an effective angle of 55.4º (from zenith), which was calculated following the procedure described by Niclòs et al. (2005). The surface effective emissivity for each site was determined using the Vegetation Cover Method (VCM, Valor y Caselles 1996) and is defined as $\varepsilon_i = \varepsilon_{i,v} FVC + \varepsilon_{i,bg}(1-FVC) + d\varepsilon_i$, where the first two terms correspond to the direct emission of the vegetation and bareground components and the last one to the cavity term that is associated with first-order reflections in the cavities defined by the rough surface. The required vegetation and bareground emissivities, $\varepsilon_{i,v}$ and $\varepsilon_{i,bg}$, were obtained by using the Box Method of Rubio et al. (1997). Table 2 shows these component emissivities and the effective emissivities determined by the VCM for both zones. Finally, LSTs were retrieved from the data measured at these stations using equation (6).

Zone	θ	FVC	Vegetation	Bareground	ε_v	ε_s	ε
A	20º	0.6	*Rosmarinus officinalis* L. & *Ulex parviflorus* L.	70% Chromic Luvisol + 30% Lithic Leptosol	0.984±0.007	0.956±0.009	0.986±0.007
	55º	0.95					0.989±0.008
B	0º	1	Rice	-	0.985±0.005	-	0.985±0.005

Table 2: **Emissivities (8-14µm) obtained for zones A and B.**

As the proposed algorithm (eq. 5) requires water vapour (W_0) as an input, a first algorithm validation was carried out using just MSG-SEVIRI images concurrent with MODIS overpasses, since W_0 can be obtained from MODIS imagery (MOD05 product). The LSA SAF algorithm does not have a direct

dependence on W_0 (eq. 2), but an estimate of W_0 is also required for the assignation of suitable coefficients.

59 concurrent MSG-SEVIRI and MODIS W_0 cloud-free images (from August to October of 2008) were first selected for the validation. LSTs obtained from the LSA SAF LST product and those by using the proposed algorithm were compared with ground-truth LSTs measured in zone A, i.e., $LST_{algorithm}$-LST_{ground_truth} differences were calculated (see Table 3). Unfortunately, there were not enough concurrent cloud-free ground-truth and MODIS data over zone B during the maximum vegetative rice growth period (when the area is most homogeneous). The results show that the proposed algorithm gives a bias of 0.7K and a standard deviation (σ) of ±1.2K, and thus a root-mean-square error (RMSE) of ±1.4K. The LSA SAF LST product shows a bias and σ of 1.5K and ±1.3K, and thus a RMSE of ±2K.

An estimate of W_0 can also be obtained by using NCEP Reanalysis data interpolated for the MSG-SEVIRI acquisition time (http://dss.ucar.edu/datasets/ds083.2/data/). A comparison of concurrent W_0 values obtained from MOD05 images and NCEP interpolated data showed a bias of 0.13cm^{-1} and a σ of ±0.3cm^{-1}, with a final RMSE of ±0.3cm^{-1}. Using these W_0 estimates, LST can be retrieved by the proposed algorithm for any cloud-free MSG-SEVIRI image without limiting them to the MODIS acquisition times, i.e. every 15 minutes. Now, biases of 0.6K and 1.6K are obtained for our algorithm and the LSA SAF product, respectively, and a σ around ±1K is shown in both cases, leading to RMSEs of ±1.2K and ±1.9K, respectively (Table 3).

Finally, 89 cloud-free matchups were additionally selected to test the algorithms in zone B by using NCEP W_0 data. In this case, biases of around -0.1K are obtained for both algorithms and σ values of ±0.9K and ±1K are shown for the proposed algorithm and the LSA SAF LST product, leading to RMSEs of ±0.9K and ±1K, respectively. Zone B is an extremely homogeneous area with a full vegetation cover of rice crops (Coll et al. 2005), and in such an "ideal" site both algorithms seem to work similarly well. However, in zone A, where the bareground-vegetation structure is more complex and the thermal diurnal variability is larger (LST_{max}-LST_{min} close to 25ºC), the results are relatively better for the proposed algorithm than for the LSA SAF LST product.

Nevertheless, more validation sites, i.e. with different geographic locations, observation angles, water vapour conditions, land cover types, and also with different levels of homogeneity, should be used to study the soundness of these algorithms thoroughly.

	(1) Zone A , W_0 (MODIS)		(2) Zone A , W_0 (NCEP)		(3) Zone B , W_0 (NCEP)	
LST algorithm	Proposed algorithm	LSA SAF	Proposed algorithm	LSA SAF	Proposed algorithm	LSA SAF
Bias (K)	0.7	1.5	0.6	1.6	-0.14	-0.08
σ (K)	1.2	1.3	1.0	1.1	0.9	1.0
RMSE (K)	**1.4**	**2.0**	**1.2**	**1.9**	**0.9**	**1.0**
N. events	59	59	527	527	89	89

Table 3: **Validation results for: (1) zone A using W_0 estimated by MODIS (MOD05), and (2) zone A and (3) zone B using W_0 obtained from NCEP data.**

CONCLUSIONS

Several topics have been investigated with the aim of improving LST retrievals from MSG-SEVIRI data in Eastern Spain. After observing classification errors in the land cover maps used by the LSA SAF to estimate the surface emissivity in our region, we suggest the generation of periodic and regional land cover maps by using a selection of representative and tested CORINE polygons and MODIS MCD43A1 images. Our preliminary results from carrying out angular measurements of surface emission show that there is an emissive angular dependence for some surfaces, such as bare soil, that should be taken into account in LST retrievals from satellite data. Furthermore, the validation of satellite-retrieved LSTs by comparison with ground-truth data measured by the two fixed stations set up in Eastern Spain shows accuracies higher than ±1.5K for the quadratic split-window equation proposed for the MSG-SEVIRI and near ±2K for the LSA SAF MSG LST product, which has apparently improved since the radiance definition change in the MSG Level 1.5 product.

ACKNOWLEDGMENT

This work has been supported by the Spanish *Ministerio de Ciencia e Innovación* (projects CGL2007-65774/CLI, CGL2008-04550, CGL2005-03386, and CONSOLIDER-INGENIO 2010 CSD2007-00067, as well as the *Juan de la Cierva* Research Contract of Dr. R. Niclòs, which is co-funded by the European Social Fund) and the European Union (Project CIRCE No. 036961). Fundación CEAM is supported by the Generalitat Valenciana and BANCAIXA.

REFERENCES

CEC (Commission of the European Communities), (1995), CORINE Land Cover Technique Guide, pp. 1-163.

Coll, C., and V. Caselles, (1997), A split-window algorithm for land surface temperature from Advanced very high resolution radiometer data: Validation and algorithm comparison, Journal of Geophysical Research, **102**(D14), pp. 16697-16713.

Coll, C., V. Caselles, J.M. Galve, E. Valor, R. Niclòs, J.M. Sánchez, and R. Rivas, (2005), Ground measurements for the validation of land surface temperature derived from AATSR and MODIS data. Remote Sensing of Environment, **97**, pp. 288-300.

Galve, J.M., C. Coll, V. Caselles, and E. Valor, (2008), An atmospheric radiosounding database for generating land surface temperature algorithms. IEEE Transactions on Geoscience and Remote Sensing, **46**(5), pp. 1547-1557.

García-Haro, F.J., S. Sommer, and T. Kemper, (2005), Variable multiple endmember spectral mixture analysis (VMESMA), International Journal of Remote Sensing, **26**, pp. 2135-2162.

Lagouarde, J.P., Y.H. Kerr, and Y. Brunet, (1995), An experimental study of angular effects on surface temperature for various plant canopies and bare soils, Agricultural and Forest Meteorology, **77**, pp. 167-190.

Madeira, C. (2002), Generalized split-window algorithm for retrieving land surface temperature from MSG/SEVIRI data, in Proceedings of Land Surface Analysis SAF Training Workshop, Lisbon 8-10 July, pp. 42-47.

Niclòs, R., V. Caselles, C. Coll, E. Valor, and J.M. Sánchez, (2005), In situ surface temperature retrieval in a boreal forest under variable cloudiness conditions, International Journal of Remote Sensing, **26**, pp. 3985–4000.

Niclòs, R., V. Caselles, C. Coll, and E. Valor, (2007), Determination of sea surface temperature at large observation angles using an angular and emissivity dependent split-window equation. Remote Sensing of Environment, **111**, pp 107-121.

Niclòs, R., M.J. Estrela, J.A. Valiente, M.J. Barberà, (2008), An angular and emissivity dependent algorithm to determine sea surface temperature from MSG-SEVIRI data, in Proceedings of the 2008 EUMETSAT Meteorological Satellite Conference, Darmstadt, Germany, 8 -12 September.

Niclòs, R., M.J. Estrela, J.A. Valiente, and M.J. Barberà, (2009), "Generación de mapas de usos de suelo periódicos a escala regional con imágenes MODIS: aplicación a la Comunidad Valenciana", in Proceedings of the "XIII Congreso Nacional de la Asociación Española de Teledetección", pp. 213-216 (only in Spanish).

Rubio, E., V. Caselles, and C. Badenas, (1997), Emissivity measurements of several soils and vegetation types in the 8-14µm waveband: analysis of two field methods, Remote Sensing of Environment, **59**, pp. 490-521.

Trigo, I.F., L.F. Peres, C.C. DaCamara, and S.C. Freitas, (2008), Thermal Land Surface Emissivity retrieved from SEVIRI/Meteosat, IEEE Transactions on Geoscience and Remote Sensing, **46**, pp. 307-315.

Valor, E., and V. Caselles, (1996), Mapping land surface emissivity from NDVI: Application to European, African and South American Areas, Remote Sensing of Environment, **57**, pp. 167-184.

Wan, Z., and J. Dozier, (1996), A generalized split-window algorithm for retrieving land surface temperature from space, IEEE Transactions on Geoscience and Remote Sensing, **34**, pp. 892-905.